



# MODELING INTERFACES AND BONDED JOINTS

H. de Boer\*, A.P.D. Weustink\*, A. Beukers\*\*, S. Koussios\*\*

\*Advanced Lightweight Engineering, \*\*Delft University of Technology, Faculty of Aerospace Engineering, Design and Production of Composite Structures

**Keywords:** *Damage, Bonded Joint, Delamination, Debonding, FEM, Interface*

## Abstract

*The present paper deals with the development of a unified model to simulate progressive failure of interfaces and adhesively bonded joints. The present damage model is capable to accurately predict both failure initiation and final failure. The model has been implemented in the commercial FE package Abaqus by means of the user subroutine UINTER. During the development, ease of use, efficiency and mesh-insensitivity have been major points of concern.*

*The unique aspect of the present approach is that no separate mixed mode law is introduced to describe mixed mode behavior. Using the actual stiffness of the interface instead of using a dummy stiffness plays here a crucial role*

*The effectiveness of the present approach is illustrated by means of several examples including a realistic industrial case study.*

## 1 Introduction

In modern aircraft fuselage design advanced composite materials are increasingly utilized. Application of bonded instead of riveted joints is also significantly increasing in aircraft design. Over the years Advanced Lightweight Engineering (ALE) has accumulated unique expertise in numerical damage modeling of Fiber Metal Laminates (FML) such as GLARE®, which is used as skin material in the new Airbus A380. These models have been developed in ABAQUS and include delamination, fiber/matrix failure, fracture energies, temperature effects, etc. This paper deals with a unified numerical approach to model both interfaces and adhesively bonded joints.

The paper is organized as follows: firstly, a short description of the applied numerical model will be presented. Several aspects, such as influences of the stiffness of the adhesive, geometrical aspects and

mixed mode behavior will be discussed. Secondly, some examples will highlight the efficiency and effectiveness of the proposed model. Finally, conclusions and recommendations will be given.

## 2 Damage modeling

Delamination occurs in the resin rich interface layer between two plies. Debonding obviously takes place in the bondline, which is normally relatively thin. There are three ways to model such layers. Either the actual layer can be modeled by means of continuum elements. However, since the layer is very thin, the number of elements needed would be very large and as such this method is rarely used in finite element analyses. A method which is frequently used in the modeling of the resin rich layer is by lumping the behavior of the layer in zero-thickness interface elements [1]. In these elements only the aspect ratio between the length and the width of the element have to be taken into account, so the number of elements is defined by the element size in the individual plies and not by the thickness of the resin-rich interface layer. A disadvantage however, is that the FE meshes of two adjacent plies have to comply so that the interface elements can be placed in between. A method that solves this last disadvantage is the modeling of the delamination behavior as an interaction law between two adjacent plies. This can be done for example in the FE package Abaqus. In this method no elements have to be generated between two layers by the user. The package itself finds the displacements between two adjacent points on the surfaces of the layers and these displacements can be used in a user defined interaction law.

Both plasticity [2], [3] and damage formulations [1], [4] can be used to model debonding phenomena. In this research a strain-based continuum damage formulation will be utilized for three reasons:

1. A strain-based formulation is more straightforward in a finite element code, since the strains are input in a FE analysis. In a plasticity formulation stresses have to be estimated based on the previous state of the material or on the elastic material and internal iterations are needed to update the stresses after increased plasticity. In a strain-based damage formulation the stresses are calculated with the current state of the material and no internal iterations are required. This makes a strain-based damage formulation less computationally expensive
2. Within a plasticity formulation it is not easy to distinguish between different softening behavior in different material directions. In a damage formulation, the different damage parameters can be easily utilized in different material directions, since individual terms in the stiffness tensor can be multiplied with independent damage parameters
3. For debonding, a damage approach is physically more realistic since degeneration of the material indeed happens through the formation of micro-cracks in the material, which grow to macro-cracks.

After damage initiation, degradation of the material parameters occurs gradually and most sources found in literature use some energy based criterion, for example based on fracture energy, for the degradation law [1],[4], [5]. For the description of delamination in this research a strain-based damage approach will be utilized in a user supplied interaction law in Abaqus. After delamination onset, a gradual degradation of the interface properties is used based on fracture energy.

Section 2.1 provides a general description of the adopted damage formulation for interfaces and bonded joints. Section 2.2 will address some issues related to modeling initial delaminations and contact. A selection of possible degradation laws is presented in Section 2.3. The Mixed Mode behavior of the present damage formulation is discussed in Section 2.4.

## 2.1 General formulation

An orthotropic delamination model, describing mixed mode delamination, is applied. The delamination model has been implemented in ABAQUS, using the surface-to-surface contact option. By using this option, the FE meshes of adjacent layers do not need to be identical. The contact algorithm of

ABAQUS will determine which node of the master surface is in contact with a given node on the slave surface. The relative displacement between these two nodes is given in a local coordinate system. The first component of the relative displacement  $u_1$  corresponds to the normal direction of the master surface. The other two components ( $u_2$  and  $u_3$ ) are the two shear components. The ABAQUS user-subroutine UINTER is used to specify a dedicated relation between the relative displacement and the corresponding traction forces. Hence, the user can define the interaction between the two surfaces.

Failure in this model is judged based on a failure function  $f$  defined as

$$f = \sqrt{\left(\frac{u_1}{u_{\max,1}}\right)^2 + \left(\frac{u_2}{u_{\max,2}}\right)^2 + \left(\frac{u_3}{u_{\max,3}}\right)^2}, \quad (1)$$

where  $u_{\max,1}$  is the gap opening displacement leading to failure and  $u_{\max,2}$  and  $u_{\max,3}$  denote the maximum shear displacement. Failure will occur when  $f > 1$ . Notice that the failure function is based on relative displacements. The stiffness of the interface is defined by the actual stiffness of the interface material. The strength of the interface is taken from experimental results. This leads to

$$u_{\max,1} = \frac{\sigma_{t,\max}}{E/t}, \quad u_{\max,2} = u_{\max,3} = \frac{\tau_{\max}}{G/t}. \quad (2)$$

Here  $t$  denotes the thickness of the interface,  $E$ ,  $G$  and the maximum allowable stresses relate to the interface material. In case of damage the elastic properties of the interface will reduce.

Now, damage parameters  $d_i$  can be defined for each direction. These damage parameters will have a value of 1 for the undamaged state and will be gradually reduced to zero in case of complete failure of the interface. The exact formulation of different choices for these damage parameters will be discussed in Section 2.3. Obviously, the damage parameters will depend on the actual value of the failure function  $f$  and on the fracture energy of the interface.

As mentioned before, the stiffness of the interface depends on the mechanical properties of the interface material itself. It is quite common in delamination modeling to use a so-called dummy stiffness for the interface. This stiffness is normally taken as high as possible without entering into numerical problems. However, this approach is not followed here. In Section 2.4 this issue will be

discussed in more detail. Using the actual material data, the modulus stiffnesses read

$$C_{11} = \frac{E}{t}, C_{22} = \frac{G}{t}, C_{33} = \frac{G}{t}. \quad (3)$$

The relation between relative displacements and tractions is given by

$$\begin{bmatrix} t_1 \\ t_2 \\ t_3 \end{bmatrix} = \begin{bmatrix} d_1 C_{11} & 0 & 0 \\ 0 & d_2 C_{22} & 0 \\ 0 & 0 & d_3 C_{33} \end{bmatrix} \begin{bmatrix} u_1 \\ u_2 \\ u_3 \end{bmatrix}. \quad (4)$$

Notice that the failure function  $f$  (Eq. 1) and the damage parameters  $d_i$  cannot be chosen independently, since

$$\int_{u_1=u_{\max}}^{\infty} t_1 du_1 = G_{c,1} \quad (5)$$

must hold true. Here  $G_{c,i}$  denotes the fracture energy per unit area for Mode I. A similar relation applies for  $G_{c,2}$ , being the fracture energy for Mode II.

## 2.2 Initial delaminations

If an initial delamination exists this delamination may close under the applied load. To prevent the two adjacent plies from penetrating, a simple contact model is utilized. In this contact model the normal stiffness of the interface is given a penalty value if the relative normal displacement between two adjacent plies is negative. The normal stiffness is zero if opening of the initial delamination occurs. The shear stiffness of the initial delamination zone is always taken equal to zero, so no friction is modeled.

## 2.3 Degradation laws

The four different softening models discussed here are:

1. Perfectly plastic. After damage initiation, the stresses in the interface do not increase any more, but remain constant upon further loading. Section 2.3.1 describes this model in more detail.
2. Linear. The interface behaves linear elastic before damage initiation. After damage occurs, the softening branch is linear too, see section 2.3.2.
3. Exponential. Again, the interface is linear elastic till damage occurs. After damage initiation, the softening branch is an exponential decay. This model is described in Section 2.3.3.

4. Smooth. In literature convergence problems were reported due to the discontinuity occurring in models 2 and 3 at damage onset. Therefore, this third model utilises a smooth behaviour of the interface. The model is described in Section 2.3.4.

All four models listed above have been implemented in UINTER.

### 2.3.1 Perfectly plastic

As mentioned before, several different degradation strategies can be applied depending on the formulation of the damage parameters  $d_i$ . The simplest formulation is obtained by defining

$$d_i = \frac{1}{f}. \quad (6)$$

Here  $f$  is defined in Eq. 1. Using the above formulation, results in a perfectly plastic behavior of the interface. Obviously, such a behavior has no real physical relevance, since final failure will never take place. Using Eq. 6 also results in violation of the constraint defined in Eq. 5.

### 2.3.2 Linear

A more useful formulation is found by defining  $d_i$  as follows

$$d_i = \frac{1}{f} \{1 - \alpha_i (f - 1)\}, \quad (7)$$

where  $\alpha_i$  is defined as

$$\alpha_i = \frac{1}{2} \frac{C_{ii} u_{\max,i}^2}{G_{c,i}}. \quad (8)$$

This formulation yields a linear degradation after damage initiation and fulfills the constraint set by Eq. 5. From Eq. 8, it is clearly seen that the parameters  $\alpha_i$  depend on the actual properties of the interface, i.e. its stiffness and fracture energy. A visualization of the corresponding behavior is depicted in Fig. 1.

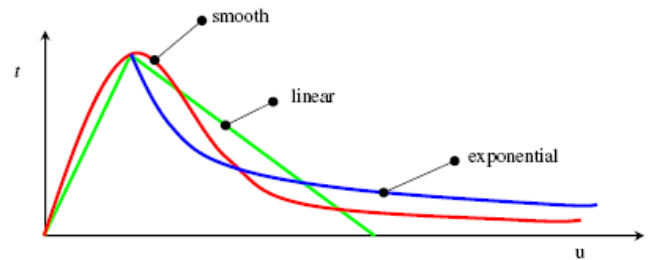


Fig. 1. Visualization of different degradation laws

### 2.3.3 Exponential

Exponential degradation of the interface is obtained by formulating the damage parameters as

$$d_i = \frac{1}{f} e^{(-\alpha_i(f-1))}, \quad (9)$$

and corresponding  $\alpha_i$  are given by

$$\alpha_i = \frac{C_{ii} u_{\max,i}^2}{G_{c,i}}. \quad (10)$$

Again, parameters  $\alpha_i$  account for the properties of the interface under consideration. A graphical presentation of the exponential degradation is given in Fig. 1. An advantage of the exponential degradation over the linear degradation is that in practice this formulation is more robust from a convergence point of view.

### 2.3.4 Smooth

A completely smooth behavior can also be obtained, see Fig.1. The advantage lies in the fact that problems related to numerical convergence around the point of damage initiation is solved rigorously. Another advantage is that mesh-sensitivity issues largely disappear due to the hardening behavior before damage initiation. A disadvantage is that the model is nonlinear from the start of the analysis, leading to more increments. The other models presented only show nonlinearity after damage initiation, which means that undamaged nodes behave linear elastic.

The formulation starts with a slightly different formulation of the displacements leading to failure (see also Eq. 2):

$$\begin{aligned} u_{\max,1} &= e^{\frac{1}{\beta} \frac{\sigma_{t,\max}}{C_{11}}}, \\ u_{\max,2} = u_{\max,3} &= e^{\frac{1}{\beta} \frac{\tau_{\max}}{C_{22}}}. \end{aligned} \quad (11)$$

Here the parameter  $\beta$  is a measure for the toughness of the interface and can be calculated as a function of the interface stiffness, strength and fracture energy.

Damage parameters are now defined as

$$d_i = e^{-\left(\frac{f^\beta}{\beta}\right)}. \quad (12)$$

The formulation presented in Eq. 11 and 12 was found to be the most useful one, since it combines accuracy, efficiency and mesh insensitivity.

### 2.4 Mixed Mode behavior

For all of the formulations (except for the perfectly plastic formulation given in Eq. 6) the behavior of the interface or adhesive joint is completely defined by the following parameters:

- Stiffness of interface material
- Thickness of the interface
- Fracture energy for Mode I and Mode II
- Peel and shear strength of interface

Hence, no additional information on Mixed Mode behavior has to be defined. Normally, a special Mixed Mode law is utilized to describe the mixed mode behavior. It will be shown that using the actual stiffness of the interface (instead of a so-called dummy stiffness) plays a crucial role in the mixed mode behavior of the interface.

### 2.5 Discussion

Damage models were presented to simulate progressive failure of interfaces in composite materials. Several degradation laws are defined. As will be shown in subsequent sections, the differences between the approaches are mostly related to numerical issues, such as convergence and mesh sensitivity. The smooth model requires in general more increments since it is nonlinear from the start of a simulation. However, this model is found to be most robust and shows nearly no mesh sensitivity.

## 3 Code validation examples

The present section presents three examples to illustrate the effectiveness of the interface models and to validate the implementation. A well-known NAFEMS benchmark is given in Section 3.1. Mode I and Mixed Mode simulations are discussed in Section 3.2 and 3.3, respectively.

### 3.1 NAFEMS Benchmark

The developed models described above are applied in the simulation of a benchmark example. The example is chosen as the NAFEMS Benchmark for composite delamination number 1A.

The benchmark deals with an isotropic circular plate loaded by a single point load at the centre. A circular delamination is assumed to start in the centre and midsurface of the plate. The size of the initial delamination and the plate, and the support conditions are arbitrarily. Failure should be unstable propagation.

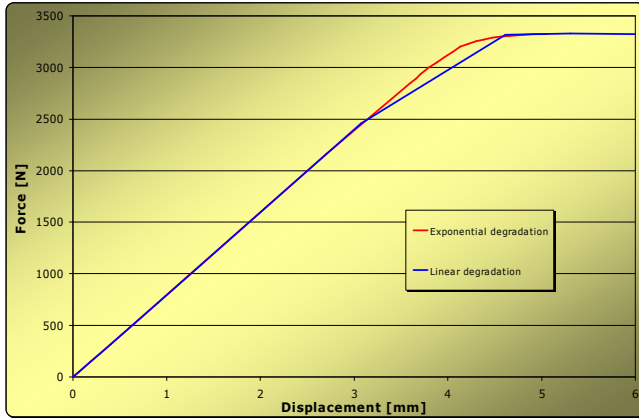


Fig. 2. Numerical results for NAFEMS benchmark problem

The results for the smooth degradation model are not included in the figure, since they follow exactly the same curve as the model utilizing exponential degradation. All models gave the same results (the difference in the figure is due to the fact that the linear model needed fewer increments)

Regarding the performance of the different models, it can be concluded that in this particular example (dealing with pure Mode II delamination), the linear degradation model shows the best convergence behaviour, although the difference with exponential degradation is only minor. The smooth model, however, needed more increments to converge, mainly due to the fact that it is nonlinear from the start. For all models, the convergence improves by using the line-search algorithm in Abaqus.

Numerical results obtained are in perfect agreement with the analytical solution for the present benchmark. Failure load for this specific case must be constant after damage initiation and should be equal to

$$P^2 = \frac{8\pi^2 E t^3}{9(1-\nu^2)} G_{II}. \quad (13)$$

Here  $P$  is the critical force,  $E$  and  $\nu$  refer to material properties of the plate,  $t$  is the thickness of the plate and  $G_{II}$  the fracture energy of the interface. For the present benchmark, the critical load is found to be 3400 N.

### 3.2 Mode I test

Fig. 3 shows a schematic representation of the Mode I test. A sheet of Fibre Metal Laminate (FML) is glued in between two thicker sheets of Aluminium

7075. Between two FML layers a Teflon insert is laminated, which will be referred to as the initial crack. A force  $F$  is applied to start the peel test. The initial crack will be extended by roughly 15 mm, which will be referred to as the pre-crack. After pre-cracking the force is released. Then, the actual testing will start by reapplying the force till a total crack length of approximately 100 mm is reached. During that phase, the cross-head displacement and the force are recorded, resulting in load-displacement graphs.

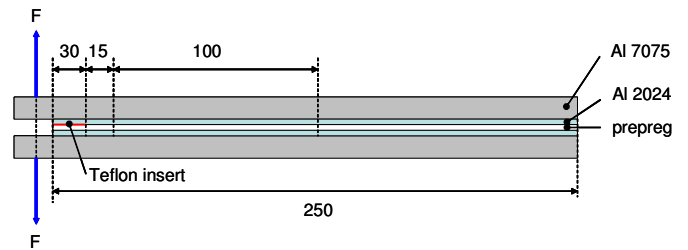


Fig. 3. Schematic representation of Mode I test. All dimensions are in mm. The width of the specimen equals 25 mm

The measured fracture energy per unit area follows from the shaded area (see Fig. 4) divided by the total area that is cracked during the actual testing. Thus, the total cracked area is calculated from the final crack length minus the pre-crack length multiplied by the width of the specimen.

The two outer layers of Al 7075 have a thickness of 4.3 mm and are added to increase the bending stiffness of the specimen. Without these layers significant plastic deformation will be found during testing which disturbs sound measurement of fracture energy.

Within in FE model, the specimens are modelled using so-called incompatible mode solid elements (C3D8I). Each layer of FML is modelled individually. Between adjacent layers debonding may occur, which is taken into account by applying the subroutine UINTER. The most important material properties for the present simulations are obviously the fracture energy  $G_I$  and the strength of the interface.

The simulation starts with an initial crack length that is equal to the length of the pre-crack, i.e. the length of the Teflon insert plus 15 mm. The load is applied by defining a prescribed displacement at the location where the force acts during the test. For reason of symmetry, only half the width of the specimen is modelled. A picture of the applied mesh is given in Fig. 5.

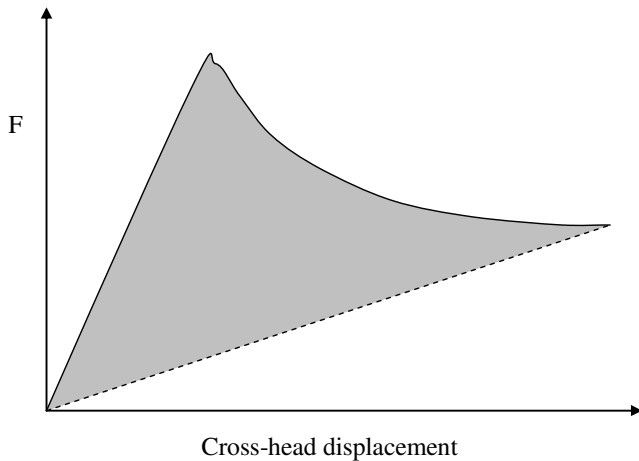


Fig. 4. Calculation of Mode I fracture energy.  $G_{I1}$  is equal to the shaded area divided by total cracked area.

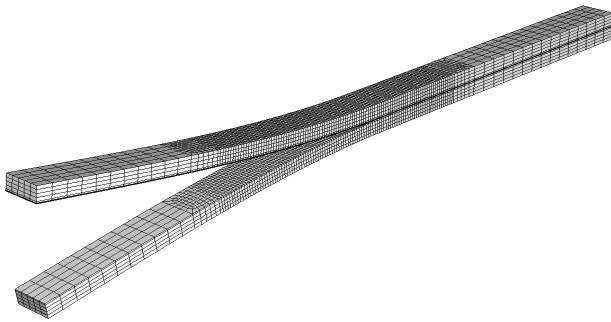


Fig. 5. Deformed mesh of Mode I simulation

The load-displacement diagram of the FE simulation is depicted in Fig. 6. The value of the fracture energy used in the calculation is taken from the Mode I experiment. Same holds true for the interface peel strength. As can be seen from Fig. 6, the FE results are in good agreement with the experimental results. The value of the limit load, as well as the corresponding cross-head displacement agrees very well. Also the shape of the descending branch is accurately predicted by the FE simulation. Moreover, when recalculating the fracture energy from the area below the load-displacement diagram (as illustrated in Fig. 4), one finds a value which is exactly the input value for the calculation.

During the FE calculation the amount of “consumed” fracture energy at each integration point is stored for post-processing. The same holds true for the value of the failure criterion, which gives the opportunity to visualize the crack front, i.e. the onset of damage. The crack front and the corresponding “consumed” fracture energy for the FML specimen are given in Fig. 7 and 8, respectively. As can be seen from these figures, at the end of the analysis the

consumed fracture energy has reached its maximum value over a large cracked area.

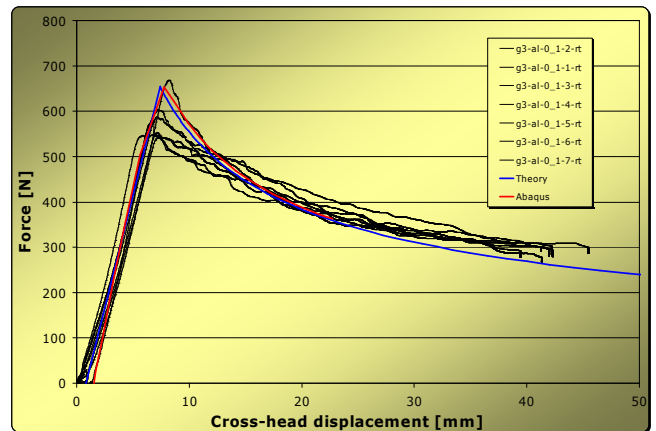


Fig. 6. Results of Mode I simulation compared to experimental results and theoretical solution

To ensure that the test really measures only Mode I fracture energy, a picture of the consumed Mode II fracture energy is given in Fig. 9. The maximum value for the consumed Mode II fracture energy is only  $3.9 \cdot 10^{-3}$  N/mm and this value is only reached at the free edges of the specimen. Hence, it can be concluded that the amount of Mode II is negligible.

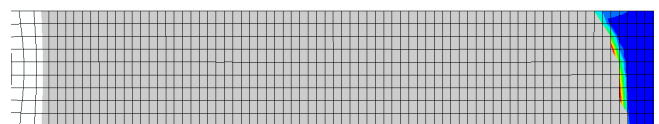
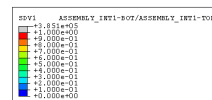


Fig. 7. Crack front at end of analysis

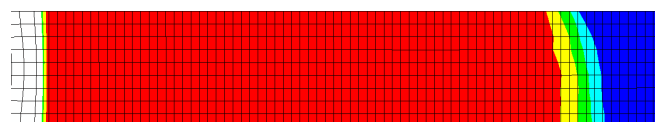
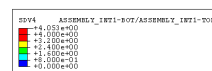


Fig. 8. Consumed Mode I fracture energy at end of analysis

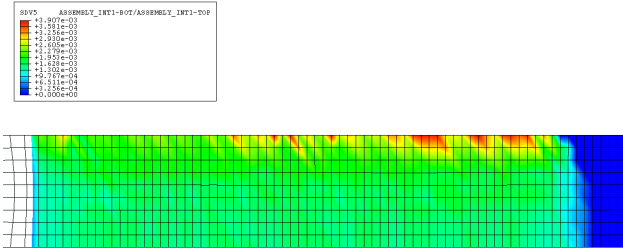


Fig. 9. Consumed Mode II fracture energy at end of analysis

### 3.3 Mixed Mode test

Since in practice delaminations in FML often initiate and propagate under the influence of combined normal and shear stresses, the third category of tests to be simulated in this work package is the Mixed Mode Bending (MMB) test (Fig. 10). During these tests, specimens are simultaneously loaded by a preset combination of both peel and shear forces. The MMB test as applied in this work package is currently a candidate for becoming an ASTM standard because of simplicity of testing and the wide range of possible mode mixtures. A schematic presentation of the test set-up is presented in Fig. 10.

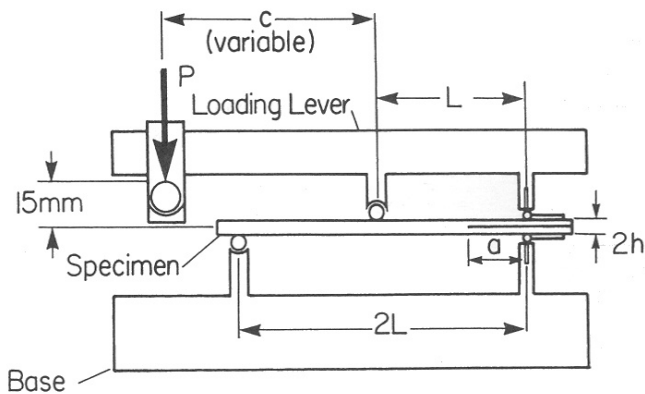


Fig. 10. Schematic presentation of Mixed Mode Bending (MMB) test set-up

By applying a load  $P$  at the indicated location the specimen, with a thickness of  $2h$  and a pre-crack that has a length  $a_0$  measured from the right support, is loaded by peel and shear stresses at the crack tip.

For each test series a specific ratio between the Mode II and Mode I is selected. This ratio depends on two parameters of the test set-up, i.e. the half span length  $L$  of the specimen and the load arm variable  $c$ , see Fig. 10. This ratio is accurately approached by the following equation:

$$\frac{G_{II}}{G_I} = \frac{3}{4} \left( \frac{c+L}{3c-L} \right)^2 \quad c \geq \frac{L}{3} \quad (14)$$

As the half span length  $L$  is the same for all specimens, the ratio can be chosen by varying the load arm  $c$ . As can be seen in the formula, the crack length  $a$  has a negligible influence on the mixed-mode ratio. During testing, a load – displacement curve is obtained. Using this data, the individual fracture toughness of the different modes can be calculated from

$$G_I = \frac{12 \cdot a_o^2 \cdot (3c-L)^2 \cdot P^2}{16b^2 \cdot h^3 \cdot E \cdot L^2} \quad (15)$$

and

$$G_{II} = \frac{9 \cdot a_o^2 \cdot (c+L)^2 \cdot P^2}{16b^2 \cdot h^3 \cdot E \cdot L^2} \quad (16)$$

The specimens are again modelled using incompatible mode solid elements. Each layer of FML is modelled individually. Between adjacent layers debonding may occur, which is taken into account by applying the subroutine UINTER.

The supports and the loading lever are modelled as rigid parts, which are in contact with the specimen, see Fig. 11. The load is applied by a prescribed displacement on the loading lever. The displacement of the loading lever at the point where the load is applied is identical to the cross-head displacement in the experiments. For reasons of symmetry, only half the width of the specimen is modelled.

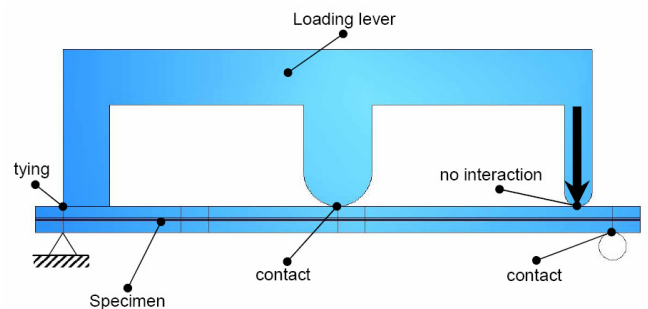


Fig. 11. Geometry and boundary conditions of Mixed Mode Bending model

For the mixed mode simulations the experimentally obtained fracture energy values for Mode I and Mode II are used. The same holds true for the peel strength and the interlaminar shear strength. Using these values a Mixed Mode test

(50% Mode I and 50% Mode II) has been analysed. Results are depicted in Fig. 12. The smooth degradation model has been utilized for the present simulations. As can be seen from the graph, the numerical results are capable to capture the actual mixed mode behaviour accurately without having specified a semi-empirical mixed mode behaviour law. Changing the stiffness of the interface and especially the ratio between normal modulus and shear modulus (depending on the Poisson ratio), significantly changes the mixed mode behaviour. Same holds true for the values of the peel strength and the shear strength. It is important to notice that the fracture energy values for Mode I and Mode II are not changed! Corresponding results are depicted in Fig. 13.

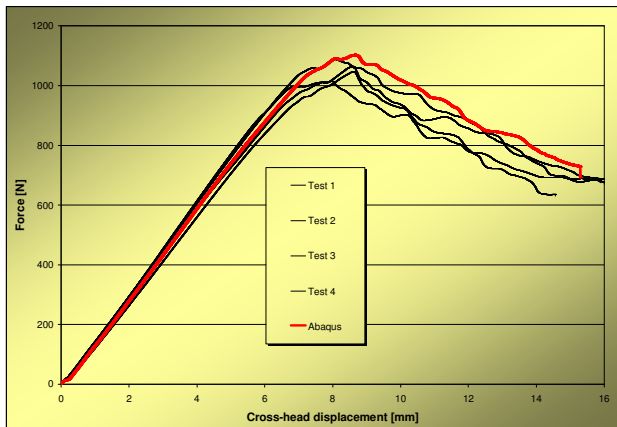


Fig. 12. FE and experimental results for 50-50 Mixed Mode test

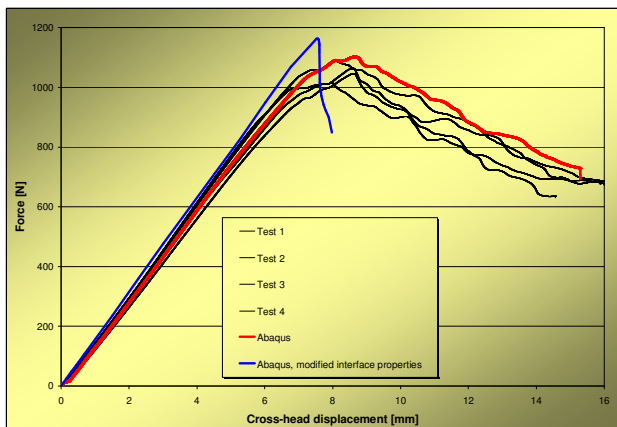


Fig. 13. Changing Poisson ratio and maximum shear strength significantly influences Mixed Mode behaviour

Investigation of the amount of the ratio between Mode I and Mode II fracture energies at limit load shows that the test is not really a 50-50 Mixed Mode test. The actual ratio between Mode I and Mode II at limit load is depicted in Fig. 14. The

figure shows the area where the ratio is between 0.75 and 1.25. Ideally, the ratio should be 1. Dark grey area at the left indicate that the amount of Mode I is larger than the amount of Mode II. Light grey areas denote that the amount of Mode II is much larger than the amount of Mode I. The change from light grey to dark grey on the right is the crack front. Thus, initially the crack initiation is dominated by Mode I, whereas after some crack propagation the crack opening is largely dominated by Mode II.

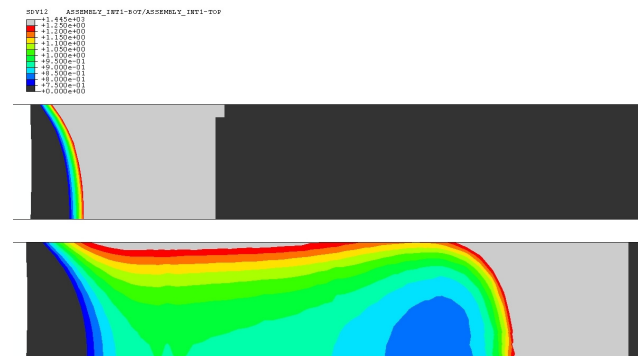


Fig. 14. Ratio Mode II/Mode I at limit load (top) and at end of analysis (bottom)

#### 4 Industrial example

The present Section shows an industrial application of the present interface models. Since details of the example are confidential information, the problem will only be discussed in general terms.

The objective of the study was to investigate the possibilities to replace an existing riveted repair method by a new bonded repair approach. An overview of the riveted repair is given in Fig. 15.

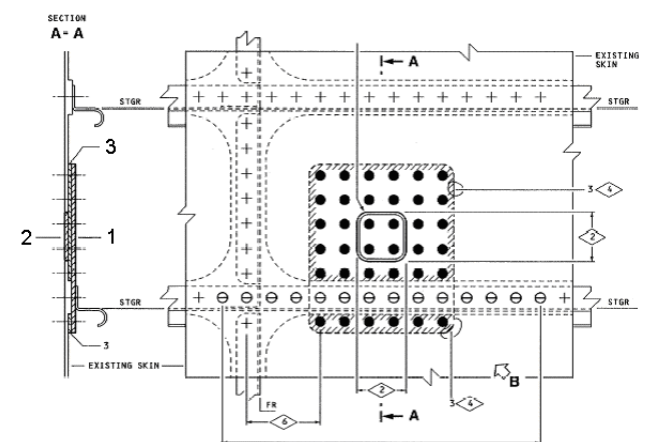


Fig. 15. Riveted repair patch on a layered aircraft structure

The problem was first analyzed in its original configuration, i.e. using rivets. Corresponding

results are depicted in Fig. 16, showing a certain measure for equivalent stresses in the doubler plate. It is clearly seen that the lower rivet row fails. According to the simulations (and confirmed by experimental evidence) failure occurs at a relatively low load.

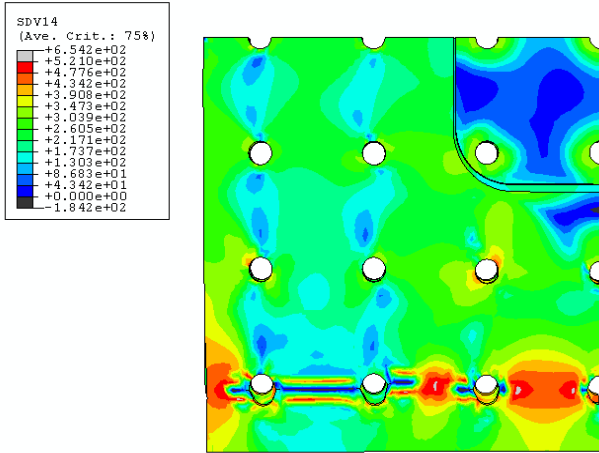


Fig. 16. Stress distribution in repair area for riveted configuration

In order to solve the problem of low failure load, and possibly to reduce weight as well, an alternative repair strategy was investigated. Here, the rivets are removed and the doubler is bonded to the damaged skin. A series of simulations have been carried out to study the effect of bondline thickness, tapering and thickness of the doubler plate. Equivalent stresses for the final optimized bonded repair are shown in Fig. 17.

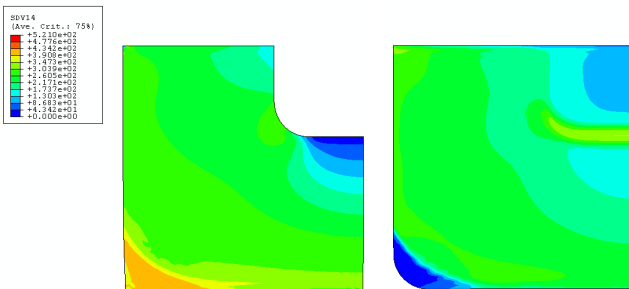


Fig. 17. Stress distribution in repair area for optimized bonded repair strategy

The failure load of the bonded repair was found to be much higher compared to the riveted repair. An increase in failure load of 25% was found. Results from tests carried out afterwards confirmed the results found by simulations. In addition, the weight of the repair has decreased by 8% due to a reduced thickness of the doubler plate.

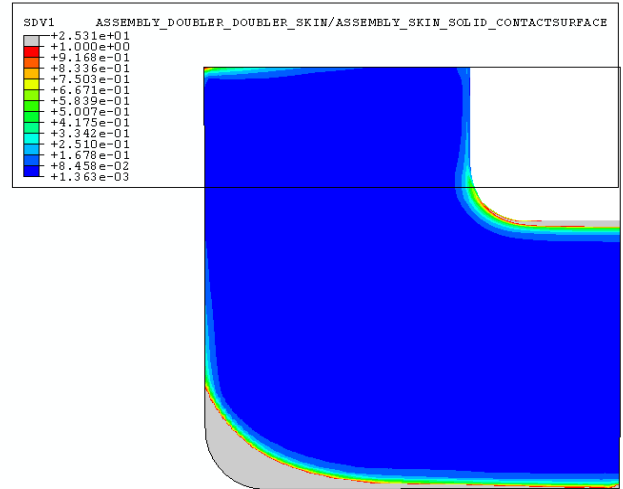


Fig. 18. Debonded area of repair after reaching failure load

### 5 Discussion and conclusions

A unified approach to simulate progressive failure of interfaces and bonded joints has been presented. The unique aspect of the present approach is that no separate mixed mode law is introduced to describe mixed mode behavior. Using the actual stiffness of the interface instead of using a dummy stiffness plays here a crucial role

Based on the results discussed in Section 3 and 4, it can be concluded that the model is able to simulate accurately and efficiently the behavior of interfaces and bonded joints.

### References

- [1] Allix, O. and Ladeveze, P. "Modelling and computation of delamination for composite laminates". *Arch. Mech.*, Vol. 44, No. 1, pp 5-13, 1992.
- [2] Schellekens, J.C.J. and Borst, R. de. "Free edge delamination in carbon-epoxy laminates: a novel numerical/experimental approach". *Comp. Struct.*, Vol. 28, pp 357-373, 1994.
- [3] Hashagen, F. "Numerical analysis of failure mechanisms in fibre metal laminates". Thesis Delft University of Technology, Delft, 1998
- [4] Daudeville, L. "Une methode simplifiee pour l'analyse du delaminage des structures composites stratifiees". Thesis universite Pierre et Marie Curie, Cachan, France, 1992
- [5] Wang, A.S.D., Sloviana, M. and Bucinell, R.B. "Delamination crack growth in composite laminates". *Proceedings of Delamination and debonding of materials*. ASTM STP 876, pp 135-167, 1985.